Journal of Zhejiang University-SCIENCE A (Applied Physics & Engineering)
ISSN 1673-565X (Print); ISSN 1862-1775 (Online)
www.jzus.zju.edu.cn; www.springerlink.com
E-mail: jzus@zju.edu.cn

Review:

Wear performance of metal parts fabricated by selective laser melting: a literature review*

Yi ZHU, Jun ZOU†‡, Hua-yong YANG

State Key Laboratory of Fluid Power and Mechatronic Systems, Zhejiang University, Hangzhou 310027, China

†E-mail: junzou@zju.edu.cn

Received June 30, 2017; Revision accepted Jan. 8, 2018; Crosschecked Jan. 15, 2018

Abstract: Selective laser melting (SLM) is one type of additive manufacturing which produces metal parts by powder bed fusion. Since the materials undergo repeated and sharp heating/cooling cycles, the SLMed parts have unique microstructures. The relations among SLM processing parameters, resultant microstructures, and mechanical properties have been investigated by many researchers. However, the wear performance of SLMed materials under various contact conditions has not been carried out until recently. This paper is a presentation of previous and recent research related to wear performance. This is a crucial aspect if SLM is to be expanded to produce friction pairs. Wear rates and mechanisms of the SLMed materials under dry, boundary lubrication, cavitation erosion, and corrosion conditions are discussed and compared with conventionally processed (CP) materials. SLMed materials benefit from fine grains and high hardness, which have higher wear resistance than CP materials. Moreover, a unique tribo-layer on the surface of the SLMed part is found to protect the bulk material under boundary lubrication conditions. An optimized combination of processing parameters increases part density, which further improves the wear resistance. Future work includes studying the influence of pores on the deforming and lubricating behaviors from dry conditions to different lubrication regimes. The final target is to actively control the processing parameters to obtain desirable material properties for improving wear performance.

Key words: Wear; Selective laser melting (SLM); Additive manufacturing; Lubrication; Pores
https://doi.org/10.1631/jzus.A1700328 **CLC number:** TH117.1

1 Introduction

In additive manufacturing, there are two main technologies which can produce metal parts by the mechanism of pre-spreading the raw materials (Uriondo et al., 2015; Zhang and Attar, 2016). One is based on metal deposition, such as laser melting deposition (LMD) (Gu et al., 2012) and wire and arc additive manufacturing (WAAM). The metal deposition process melts the powders as they are being put down. The other is based on powder bed fusion, such as electron beam melting (EBM) and selective laser melting (SLM). Fig. 1 shows the classification of metal additive manufacturing. Powder bed fusion melts materials selectively according to the pre-sliced computer aided design (CAD) model on a layer of pre-spread powders. Compared to EBM, SLM can produce parts with high accuracy and surface roughness but with a low building rate. A comparison between SLM and EBM can be found in some studies (Koike et al., 2011; Uriondo et al., 2015; Liu et al., 2016, 2017; Bai et al., 2017). In this paper, we only focus on the SLMed parts.

In the SLM, the laser power (usually 200 W or 400 W) is focused on a tiny spot with a diameter less

‡ Corresponding author

* Project supported by the National Natural Science Foundation of China (Nos. 51775486 and 51521064), the Fundamental Research Funds for the Central Universities of China (No. 2017FZA4001), and the National Basic Research Program (973 Program) of China (No. 2015CB058100)

ORCID: Jun ZOU, https://orcid.org/0000-0003-2443-3516

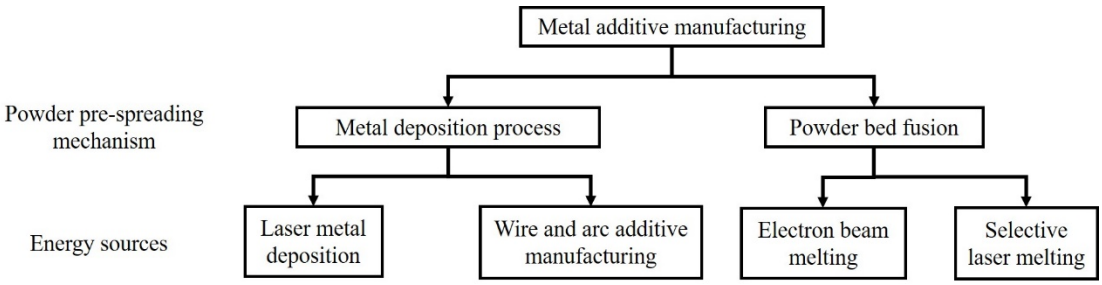

Fig. 1 Classification of metal additive manufacturing (modified from (Uriondo et al., 2015))

than 100 μm. The temperature inside the spot can be over 2000 °C while the temperature nearby is only several hundred degrees, causing huge thermal gradients. Moreover, the laser scanning speed is high from tens to thousands mm/s. In order to achieve high density, materials are re-melted while the laser scans between tracks in the same layer and between two layers, as shown in Fig. 2 (El Kadiri et al., 2008). Therefore, the materials undergo sharp and repeated heating/cooling cycles. A schematic thermal behavior in the SLM process is indicated by Li and Gu (2014), as shown in Fig. 3. The heat conduction, convection, and radiation in the SLM process is very complicated, which results in the SLMed materials with some unique characteristics. Some studies investigated the interaction between the laser and the powders (Gu and Shen, 2007; Simonelli et al., 2015; Zhou et al., 2015). Some physical phenomena, such as balling effect and laser spatter, were analyzed.

Consequently, the microstructure of the SLM parts differs from the conventional parts in terms of grain size and morphology, pores and cracks, phase, and residual stress. Different material microstructures result in different mechanical properties. Many researchers studied the influence of processing parameters on material characterization and mechanical properties. Materials include commercialized standard ones, such as AlSi10Mg (Brandl et al., 2012; Kempen et al., 2012; Thijs et al., 2013), Ti6Al4V (Bey Vrancken et al., 2012; Wu et al., 2016), 316L stainless steel (Cherry et al., 2014; Sun et al., 2016), and customized ones (Zheng et al., 2010; Gu et al., 2011a; Li et al., 2014; Vrancken et al., 2014; Attar et al., 2014a, 2014b, 2014c, 2015b; Prashanth et al., 2015; Scudino et al., 2015). In those publications, the influence of laser processing parameters on microstructure, phase evaluation, density, hardness, tensile strength, fatigue strength, etc. was often analyzed. On the other hand, some studies focused on one property based on specific applications. Hedberg et al. (2014) studied the biocompatibility of CoCrMo dental alloy. Leuders et al. (2013) and Riemer et al. (2014) focused on the crack growth behaviors for applications in aerospace and biomedical sectors. Cabrini et al.

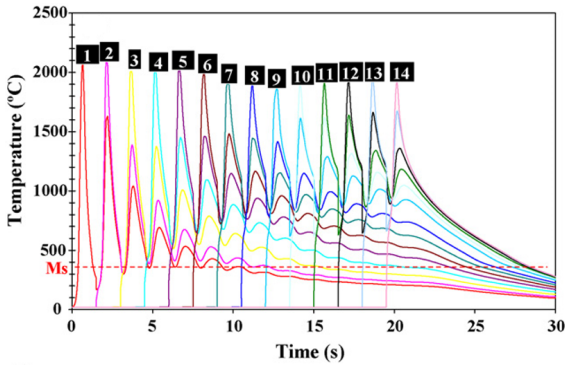

Fig. 2 Thermal history of the mid-point at each deposited layers calculated by finite element simulations. Reprinted from (El Kadiri et al., 2008), Copyright 2008, with permission from Elsevier

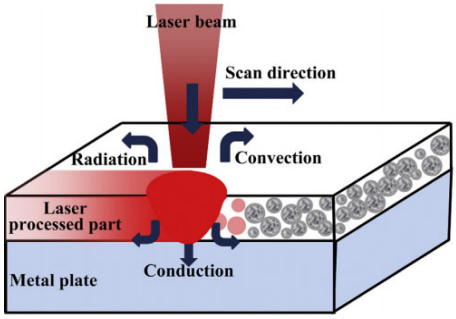

Fig. 3 Schematic of thermal behavior of powder bed under laser irradiation. Reprinted from (Li and Gu, 2014), Copyright 2014, with permission from Elsevier

(2016) and Chen et al. (2017) investigated the corrosion behaviors of additively manufactured materials.

Wear is the loss or displacement of material from a contacting surface, which constitutes the main limitation of the technical and economic service life of a machine (van Beek, 2006). Wear has various forms including adhesive wear, abrasive wear, corrosive wear, erosive wear, and fatigue. The wear mechanism greatly depends on material properties and contact conditions including contact loads, running speeds, contact temperature, environment, and lubricants. Wear studies related to industrial applications are mostly based on conventionally manufactured parts. Wear of metal parts produced by SLM is crucial since wear mechanisms must be well studied before the SLMed parts can be used in industry. In addition, the topic of wear is also interesting for biomedical applications since orthopedic implants are difficult to have replaced (Attar et al., 2014b; Ehtemam-Haghighi et al., 2017). However, studies on the wear performance of SLM parts are few. This is because most SLM parts are produced as structure parts which are free from impact and relative movements. In that case, improving material densification and strength is more important than reducing wear. On the other hand, wear resistance does not linearly relate to the part density. It greatly depends on the application and the running conditions. A 100% dense part may give a poorer wear resistance than a part which is not fully densified under certain conditions.

This review paper summarized the wear studies from published articles and some on-going work. The motivation of the paper is to highlight the importance of wear for the SLMed parts so as to expand the SLM technology to produce contacting parts. The material characteristics of the SLMed parts which might affect the contact and wear are presented. Wear behaviors and mechanisms in fretting contact, sliding contact, cavitation erosion, and corrosive wear are analyzed. Finally, future trends are discussed.

2 Selective laser melting

2.1 Machine and working process

Commercial machines based on the powder bed fusion technique are EOS, Concept laser, SLM solution, Renishaw, etc. An SLM machine usually consists of an ytterbium fiber laser, an automatic powder layering system, a gas protection system, and a process control system. A schematic of an SLM machine is shown in Fig. 4 (Zhu et al., 2016b). Different machines vary in laser power, building chamber volume, protecting gas, and powder layering pattern. However, the working principle of each is almost the same. The sealed working chamber is fed with high-purity inert gas, and the oxygen content is reduced below a certain level in order to prevent metal powders from oxidizing. A powder layer with a certain thickness is employed and each powder layer is scanned by the laser to build up the sample according to the predefined CAD model. These two steps are carried out continuously until the part is built up.

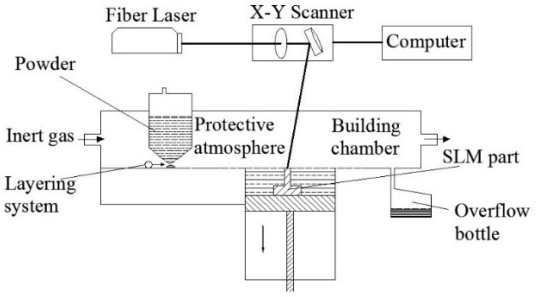

Fig. 4 Schematic of the Renishaw SLM system. Reprinted from (Zhu et al., 2016b), Copyright 2016, with permission from Elsevier

2.2 Powders and processing parameters

Metal powders are spherical in shape. The powder size of different materials varies, mostly ranging from 10 μm to 50 μm. The size distribution of metal powders is crucial since it affects the powder flowability and powder layering, which finally influences the part densification. A typical scanning electron microscope (SEM) image and size distribution of titanium powders are shown in Fig. 5.

In order to densify the metal parts, there are many laser processing parameters which can control the laser energy absorbed by powders. Processing parameters mainly include laser power, exposure time, point distance, hatching distance, layer thickness, and scanning strategy. Most parameters are illustrated in Fig. 6. Laser processing parameters and

particle shapes and sizes influence the properties of the manufactured parts (Zhang et al., 2011; Körner et al., 2013; Attar et al., 2014a, 2014b, 2015a; Liu et al., 2015). Exposure time indicates the time that the laser dwells on one spot during scanning. Layer thickness refers to the thickness of each layer by the powder layering system. Scanning strategy indicates how the laser scans each layer and multi-layers, as presented in Fig. 7. In order to evaluate the laser energy, a parameter named laser energy density is often used:

$$E\ (\mathrm{J/mm^3}) = \frac{P\ (\mathrm{W})}{h_s\ (\mathrm{mm}) \times v\ (\mathrm{mm/s}) \times l\ (\mathrm{mm})}, \qquad (1)$$

where P is the laser power, h_s is the hatch distance, v is the scanning speed defined as the point distance divided by the exposure time, and l is the layer thickness.

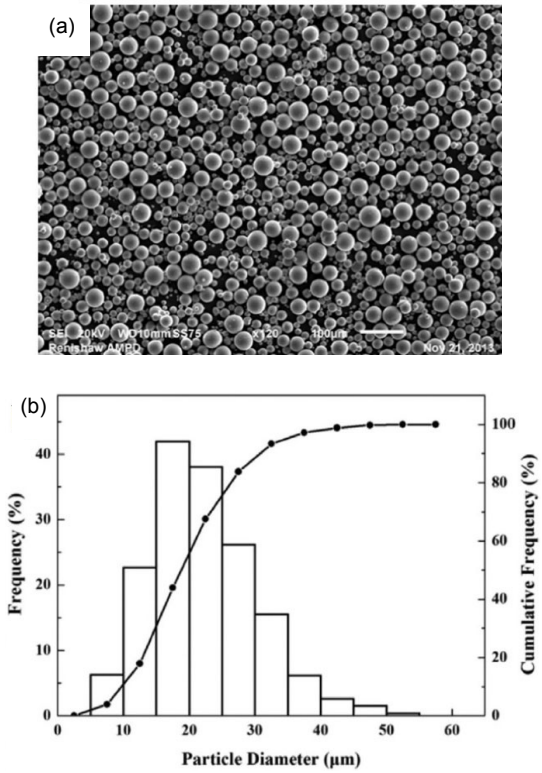

Fig. 5 SEM image (a) and size distribution (b) of Ti6Al4V powders. Fig. 5a is reprinted from (Zhu et al., 2016b), Copyright 2016, with permission from Elsevier. Fig. 5b is reprinted from (Wu et al., 2016), Copyright 2016, with permission from Elsevier

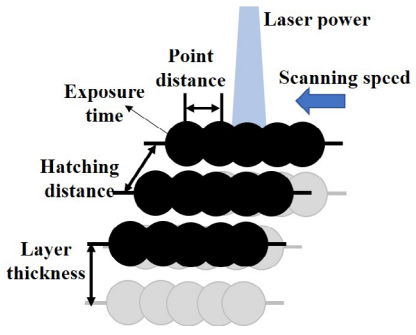

Fig. 6 Schematic of laser scanning

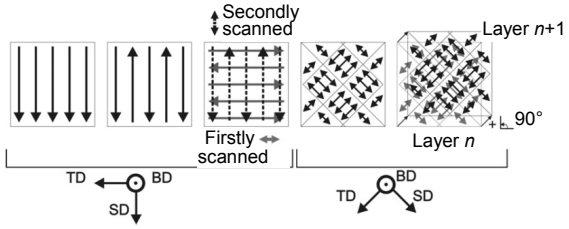

Fig. 7 Schematic of laser scanning strategy

TD, BD, and SD refer to the transverse direction, building direction, and scanning direction. Reprinted from (Thijs et al., 2013), Copyright 2012, with permission from *Acta Materialia*

3 Material characteristics

As mentioned in the introduction, SLM-made materials undergo repeated and sharp heating/cooling cycles, which makes the microstructure different. Fig. 8 shows the microstructure of 316L stainless steel produced by SLM and conventional methods (Zhu et al., 2016a). It clearly shows that the austenite grains are densely arranged in the SLMed parts and the size of the grain is much smaller than that of the conventionally processed (CP) part. Fig. 9 shows the microstructures of Ti6Al4V produced by SLM and conventional methods (Zhu et al., 2016b). The CP sample indicates a lamellar microstructure while the SLMed sample shows a fully acicular α′ martensitic microstructure. The difference in the microstructure of Al-12Si between the SLMed and CP parts was reported by Prashanth et al. (2014). Because of the difference in the microstructure and phase change, X-ray diffraction (XRD) peaks were reported to be slightly shifted and broadened (Zhu et al., 2016b). There are many studies on the influence of processing parameters (Gu et al., 2011a, 2012, 2015), building

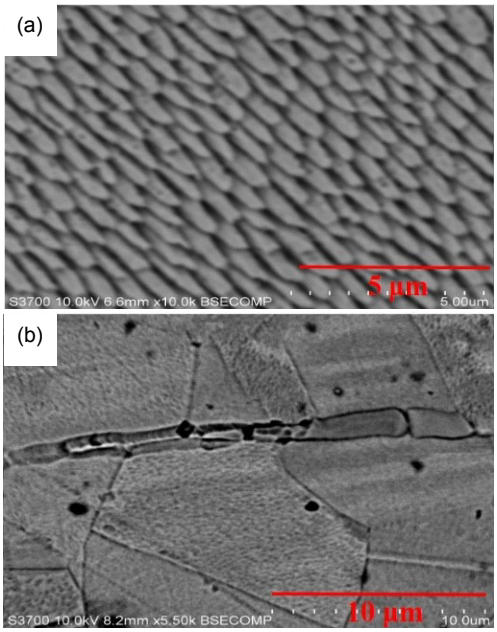

Fig. 8 SEM images showing microstructures of 316L stainless steel produced by SLM (a) and conventional process (b). Reprinted from (Zhu et al., 2016a), Copyright 2016, with permission from Elsevier

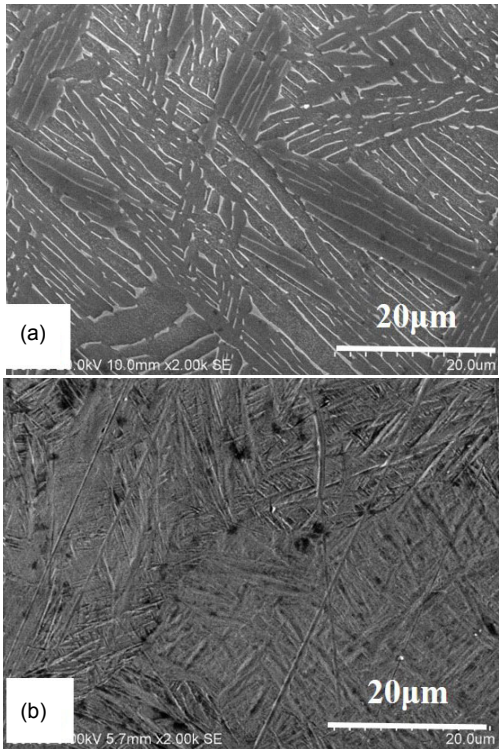

Fig. 9 SEM images showing microstructures of Ti6Al4V produced by SLM (a) and conventional process (b). Reprinted from (Zhu et al., 2016b), Copyright 2016, with permission from Elsevier

direction (Brandl et al., 2012), environmental conditions (Zhang et al., 2013), and post heat treatments (Vrancken et al., 2012; Wu et al., 2016) on the microstructure. Pores are often very common in the SLM samples (Fig. 10), particularly when the sample is not fully densified because of poor processing parameters. Pores differ in size and morphology. These differences have several causes: (1) the balling effect (Gu and Shen, 2007; Zhou et al., 2015), (2) residual oxygen in the building chamber, and (3) imperfections in the powders (Sun et al., 2016). Much effort has been made to reduce the pores since they negatively influence mechanical properties (Thijs et al., 2010; Qiu et al., 2015; Uriondo et al., 2015). On the other hand, pores are also important for tribological performance, since pores inside the sample affect plastic deformation and crack propagation. Pores on the surface also greatly affect the lubricating behavior and the local contact conditions.

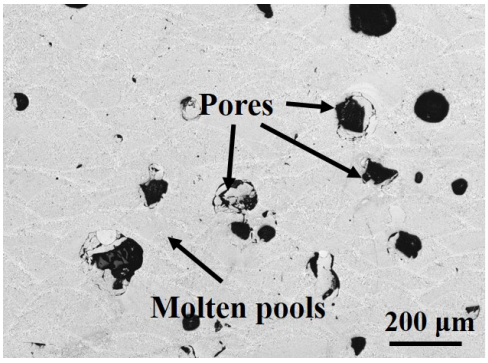

Fig. 10 Pores in the AlSi10Mg sample. Reprinted from (Zou et al., 2017), Copyright 2017, with permission from Elsevier

Another property worth mentioning is hardness, which affects wear performance. Because of smaller grains, SLMed materials are usually harder than CP materials (Manfredi et al., 2013; Jägle et al., 2014; Zhu et al., 2016a, 2016b; Zou et al., 2017). According to the Archard equation, the wear volume is inversely proportional to the hardness of the material. Thus, a harder SLMed sample generally has a higher wear resistance than the corresponding CP sample. However, the hardness varies depending on the location of the SLMed sample. Li et al. (2014) found out that hardness varied at different regions of the scan tracks

(i.e. different scanning layers in the building direction and different scanning tracks in cross section). The hardness measured near the top layer and the bottom layer is also higher than that measured in the middle part because of the difference in heat conduction (Wang and Chou, 2017).

4 Wear performance

The wear property presented in previous studies was often treated as one constituent of mechanical properties (e.g. tensile stress and hardness) of the SLMed parts. Only a few studies specifically focused on wear behaviors and mechanisms based on certain applications.

4.1 Dry wear

Kumar and Kruth (2008) pioneered the work by investigating the wear performance of various SLMed materials using dry fretting tests. The contact condition is shown in Table 1. Results show that the wear resistance of the SLMed materials is higher than the CP materials. Abrasive wear is the main cause for fretting degradation of the SLMed tool steel while excavation of wear debris is the main wear mechanism for the SLMed stainless steel. It should be noted that the microstructure is not discussed and the wear mechanisms between the SLMed and the CP samples are not compared. All the dry wear results in this section are listed in Table 1 for comparison.

4.1.1 Ti and titanium alloy

Attar et al. (2017) studied the wear properties of the SLMed Ti and Ti-TiB using a pin-on-disk rig. The wear resistance is reportedly related to the corresponding H/E_r and H^3/E_r^2 (H is the hardness and E_r is the elastic modulus) obtained by nanoindentation. Wear resistance is improved by adding TiB particles (Figs. 11 and 12). Attar et al. (2015c) compared the pure Ti prepared by SLM to cast samples. The SLMed sample has a better wear resistance under various applied loads due to martensitic microstructure, fine grain size, and superior micro hardness. Ploughing grooves and material delamination are found on both samples indicating similar wear mechanisms. Gu et al. (2011a, 2011b, 2012) studied the influence of the SLMed samples produced by different processing parameters on wear properties. Results indicate that the wear rate is related to the density and hardness. However, the difference in wear rates is not large. Ehtemam-Haghighi et al. (2016) investigated the influence of the addition of Nb on the wear resistance of Ti-xNb-7Fe and found that the wear resistance decreased with the increasing Nb concentration due to severe delamination.

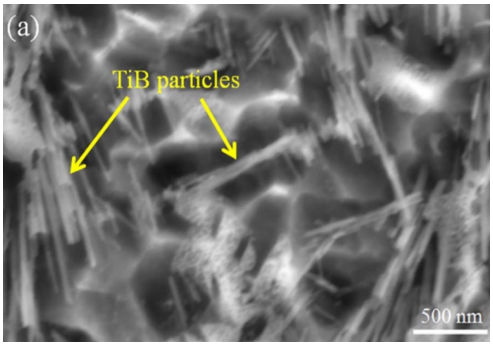

Fig. 11 SEM of Ti-TiB composite materials after SLM processing. Reprinted from (Attar et al., 2017), Copyright 2017, with permission from Elsevier

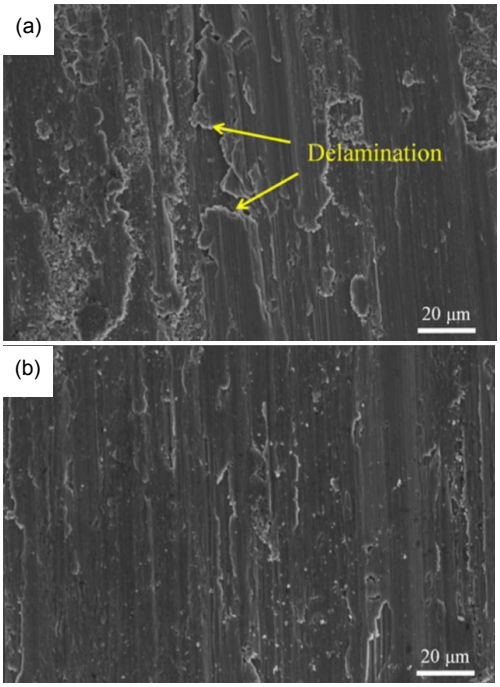

Fig. 12 SEM images of worn surfaces after wear testing of CP-Ti (a) and Ti-TiB composite materials (b) produced by SLM. Reprinted from (Attar et al., 2017), Copyright 2017, with permission from Elsevier

Table 1 Contact conditions and wear rates under dry conditions

Reference	SLMed materials/ counterbody material	Contact type	Motion	Contact pressure*	Speed (or frequency)	Wear rate** (or wear volume)	Compare to CP
Kumar and Kruth, 2008	Stainless steel/ Chrome steel	Point contact (dry)	Fretting	290 MPa, 410 MPa	10 Hz	15–39 mm^3, 51–66 mm^3	Low
	Tool steel/ Chrome steel					198 mm^3, 463 mm^3	Low
	Ti6Al4V/ Chrome steel					7362 mm^3, 9337 mm^3	No data
	CoCrMo/ Chrome steel					1474 mm^3, 2252 mm^3	No data
Attar et al., 2017	Pure Ti/ Hardened steel	Face contact (dry)	Sliding	2 MPa	0.54 m/s	5.5 μg/(m·N)	No data
	Ti-TiB/ Hardened steel					2.1 μg/(m·N)	No data
Attar et al., 2015a	Pure Ti/ Hard-faced stainless steel	Face contact (dry)	Sliding	2.1 MPa, 2.8 MPa, 3.5 MPa, 4.2 MPa	0.5 m/s	0.21 μg/(m·N), 0.26 μg/(m·N), 0.27 μg/(m·N), 0.36 μg/(m·N)	Low
Gu et al., 2011a	TiN-Ti_5Si_3 composite (disk)/ GCr15 (pin)	Point contact (dry)	Sliding	1.6 GPa	0.117 m/s	0.4 μg/(m·N) (at 2.5 kJ/m), 0.33 μg/(m·N) (at 3.3 kJ/m), 0.31 μg/(m·N) (at 5 kJ/m), 0.44 μg/(m·N) (at 10 kJ/m)	No data
Gu et al., 2012	Pure Ti (disk)/ GCr15 (pin)	Point contact (dry)	Sliding	1.6 GPa	0.117 m/s	4.9 μg/(m·N) (at 225 J/m), 3.8 μg/(m·N) (at 300 J/m), 4.0 μg/(m·N) (at 450 J/m), 5.3 μg/(m·N) (at 900 J/m)	No data
Gu et al., 2011b	TiC/ Ti5Si3 (disk)/ GCr15 (pin)	Point contact (dry)	Sliding	1.6 GPa	0.117 m/s	0.95 μg/(m·N) (at 200 J/m), 0.78 μg/(m·N) (at 267 J/m), 0.6 μg/(m·N) (at 400 J/m), 1.1 μg/(m·N) (at 800 J/m)	No data
Ehtemam-Haghighi et al., 2016	Ti-*x*Nb-7Fe (disk)/ Hard-faced stainless steel (disk)	Face contact (dry)	Sliding	0.49 MPa	0.5 m/s	<0.018 μg/(m·N)	Lower than as-cast CP-Ti
Prashanth et al., 2014	Al-12Si (pin)/ Hard-faced stainless steel (disk)	Face contact (dry)	Sliding	0.35 MPa	1 m/s	0.24–0.30 μg/(m·N) for different heat treatment temperatures	Low
	Al-12Si (disk)/ GCr15 steel (ball)	Point contact (dry)	Fretting	1.02 GPa	50 Hz	0.001–0.029 mm^3 for different heat treatment temperatures	Low
Prashanth et al., 2016	Al-12Si-TNM (pin)/ Hard-faced stainless steel (disk)	Face contact (dry)	Sliding	0.8 MPa	1 m/s	0.10 μg/(m·N), 0.16 μg/(m·N), 0.32 μg/(m·N), 0.40 μg/(m·N), 0.56 μg/(m·N)	Low

(To be continued)

(Table 1)

Reference	SLMed materials/ counterbody material	Contact type	Motion	Contact pressure*	Speed (or frequency)	Wear rate** (or wear volume)	Compare to CP
Kang et al., 2016	Al-12Si (disk)/ Al_2O_3 (ball)	Point contact (dry)	Sliding	1.08 GPa	30 mm/s	2.44 μg/(m·N) (at 160 W), 1.90 μg/(m·N) (at 195 W), 1.88 μg/(m·N) (at 210 W), 4.42 μg/(m·N) (at 225 W)	No data
Chen and Gu, 2016	4Cr5MoSiV (disk)/ GCr15 (ball)	Point contact (dry)	Sliding	1.6 GPa	0.117 m/s	5.7 μg/(m·N) (at 2400 mm/s), 2.11 μg/(m·N) (at 2000 mm/s), 1.56 μg/(m·N) (at 1600 mm/s), 3.82 μg/(m·N) (at 1200 mm/s)	No data
AlMangour et al., 2016	TiB_2 reinforced 316L (disk)/ 52100 bearing steel (ball)	Point contact (dry)	Sliding	1.6 GPa	0.176 m/s	4.9 μg/(m·N) (with 2.5% TiB_2), 3.5 μg/(m·N) (with 5% TiB_2), 0.58 μg/(m·N) (with 10% TiB_2), 0.04 μg/(m·N) (with 5% TiB_2)	Low
AlMangour et al., 2017a	TiC reinforced 316L (disk)/ GCr15 steel (ball)	Point contact (dry)	Sliding	1.6 GPa	0.117 m/s	1.17 μg/(m·N) (at 67 J/mm^3), 1.01 μg/(m·N) (at 100 J/mm^3), 1.48 μg/(m·N) (at 200 J/mm^3), 2.03 μg/(m·N) (at 300 J/mm^3)	No data
AlMangour et al., 2017b	TiB_2 reinforced 316L (disk)/ 52100 bearing steel (ball)	Point contact (dry)	Sliding	1.6 GPa	0.105 m/s	0.0043 μg/(m·N) (directly mixed), 0.0015 μg/(m·N) (ball milled), 0.77 μg/(m·N) (after HIP1), 1.26 μg/(m·N) (after HIP2)	No data
Sun et al., 2013	316L (disk)/ stainless steel (ball)	Point contact (dry)	Sliding	1.39 GPa	0.04 m/s	2.57 μg/(m·N) (at 125 mm/s), 1.64 μg/(m·N) (at 150 mm/s), 2.50 μg/(m·N) (at 175 mm/s), 5.15 μg/(m·N) (at 200 mm/s)	High
Jia and Gu, 2014	Inconel 718 (disk)/ GCr15 (ball)	Point contact (dry)	Sliding	1.6 GPa	0.117 m/s	7.64 μg/(m·N) (at 180 J/mm^3), 6.22 μg/(m·N) (at 275 J/mm^3), 4.79 μg/(m·N) (at 300 J/mm^3), 3.86 μg/(m·N) (at 330 J/mm^3)	No data
Rong et al., 2016	WC reinforced Inconel 718 (disk)/ GCr15 (ball)	Point contact (dry)	Sliding	1.91 GPa	0.117 m/s	2.44 μg/(m·N) (at 350 mm/s), 2.10 μg/(m·N) (at 450 mm/s), 2.86 μg/(m·N) (at 550 mm/s), 3.44 μg/(m·N) (at 650 mm/s)	No data

* Non-conformal contact pressure was calculated according to the maximum Hertzian contact theory (Johnson, 1985); ** Sliding wear rate was calculated as the mass loss divided by the sliding distance and applied load; HIP means hot isostatic pressing

4.1.2 Al-Si alloy

Prashanth et al. (2014) studied the wear properties of SLM-made Al-12Si samples by sliding and fretting contact. The as-prepared SLM samples, the SLM samples annealed at different temperatures, and the cast samples are compared. The wear rate is shown to be inversely proportional to the hardness, the size of Si particles, and the annealing temperature. Sliding wear result shows that the as-prepared SLMed material gives the least wear rate compared to the cast and the heat-treated SLM samples. However, the difference is small. Abrasive wear is the major wear mechanism, and oxide wear is also visible. Fretting wear tests show similar trends and the as-prepared SLM sample displays the minimum wear loss. Increased annealing temperature increases the growth of Si particles, which causes the deterioration of the wear properties reducing the resistance of the Al-12Si material against sliding and fretting wear. Prashanth et al. (2016) also reported that the wear rates of the SLMed Al-12Si-TNM samples increased with the increasing loads. Moreover, the wear rates of the SLMed composites are generally lower than those of the SLM-made Al-12Si. Kang et al. (2016) studied the wear resistance of Al-Si alloy and found that the laser power greatly influenced the wear rates.

4.1.3 Steel

Chen and Gu (2016) measured the wear rate of SLM-made 4Cr5MoSiV steel and found that the wear rate was related to the laser energy density, the resultant density, and hardness. AlMangour et al. (2016, 2017a, 2017b) investigated the wear resistance of reinforced 316L stainless steel (with TiB_2 or TiC). Results of AlMangour et al. (2016) indicated that the wear resistance increases with the increasing TiB_2 content due to combined effects of grain refinement and grain-boundary strengthening. AlMangour et al. (2017b) showed that a hot isostatic pressing (HIP) post-treatment can reduce the hardness, which greatly increases the wear rate due to the transformation of equiaxed grains into agglomerated nanoparticles. The wear rate of TiC-reinforced composites is related to the densification level and microstructural coarsening (AlMangour et al., 2017a). Decreased scanning speed results in a decreased cooling rate which leads to coarse grains. Sun et al. (2013) studied the wear rates of the SLM-made 316L stainless steel samples. Results show that the porosity of the SLMed samples is closely related to the scanning speeds, which further affects the wear rates. However, all SLMed samples have lower wear resistance than standard 316L stainless steel. It is also pointed out that fracture is the main wear mechanism and pores in SLM samples serve as crack initiation and propagation sites leading to accelerated material loss.

4.1.4 Inconel

Jia and Gu (2014) studied the influence of laser energy density of SLMed Inconel 718 on the dry sliding wear rate. They found that wear rate decreased with the increasing energy density because of the improved hardness and the formation of an adherent tribo-layer. Rong et al. (2016) further investigated the wear behaviors of the WC reinforced Inconel 718 fabricated by different laser scanning speeds. Results indicated that the samples with low laser speeds generally had low wear rates and the wear mechanism switches from severe abrasive wear to adhesive wear.

4.2 Sliding wear under lubricated conditions

Most industrial parts are lubricated in order to reduce friction and wear. The SLMed samples containing pores and cracks may give different results under lubricated conditions compared to dry contacts. However, work on this has only just started and there are few results. Zhu et al. (2016a, 2016b) performed the study specifically focused on the wear performance of the SLMed 316L stainless steel and Ti6Al4V under boundary lubrication regimes using a ring-on-disc rig. A load of 3300 N was applied which is equivalent to a contact pressure of 15 MPa (face contact) and the speed is 10 r/min. A study of 316L stainless steel (Zhu et al., 2016a) indicates that the wear rate of the SLMed samples is similar to that of the CP ones while contacting with soft materials (brass). However, the wear rate of the SLMed samples is lower than that of the CP ones while contacting with a hard material. It is found out that the fine grains of the SLMed samples improve the wear resistance. Nevertheless, the pores in the SLMed samples cause severe plastic deformation, which leads to material shell off.

Work on titanium alloy compares the as-prepared SLM samples, the heat-treated SLM samples, and the CP samples (Zhu et al., 2016b). The same contact conditions as in the previous study (Zhu et al., 2016b) were applied to this study. The wear for Ti6Al4V in contact with a soft material is characterized as mild wear. Adhesive wear prevails because of the failure of the lubricant. The tribo-layer is thin and contains a trace of oxygen. Oxidative wear, abrasion, and delamination are observed on the Ti6Al4V surface in contact with a hard material. Only the heat-treated SLM sample generates a protective tribo-layer containing oxygen without plastic deformation in the bulk material, which has the lowest wear rate, as shown in Fig. 13.

From these two studies, it can be seen that under the boundary lubrication conditions where a lubricating film is not yet formed and two surfaces bear all applied load, the SLMed samples generally have higher wear resistance than the CP samples due to closely arranged and fine grains. The SLMed samples present different wear mechanism and a different tribo-layer. It is important because SLM parts exhibit new tribological phenomena. However, it should also be noted that the SLMed samples mentioned in the references were produced by optimized laser processing parameters.

4.3 Erosive wear

Erosion refers to the material loss due to the impact of fluids at high speeds. Erosion is one type of one-body wear which is critical in fields such as hydraulics and aerospace. Zou et al. (2017) pioneered the work by studying the cavitation erosion behavior of SLMed AlSi10Mg samples. Cavitation erosion is a combined effect of cavitation and high-speed fluids. The work was performed on an ASTM G134 test rig. The pressure of the water pump was set to 16 MPa and the stand-off distance was 18 mm. The SLMed aluminum alloy samples were fabricated by various laser scanning speeds, and a wrought sample was also used to give a comparison. The mass loss behaviors of the SLMed samples greatly differ compared to the classical theory (wrought sample), as shown in Figs. 14 and 15. The cavitation erosion rate of the SLMed samples peaks at a very high level in the beginning and then decreases significantly. The erosion rate of the SLMed samples is extremely low in the steady-state period, at one tenth of that of the wrought sample. A continuous observation of surface topography finds that the high erosion rate at the beginning is due to the existence of the un-melted particles inside the pores, as shown in Fig. 16. High hardness and the fine grains of SLMed parts are considered as the

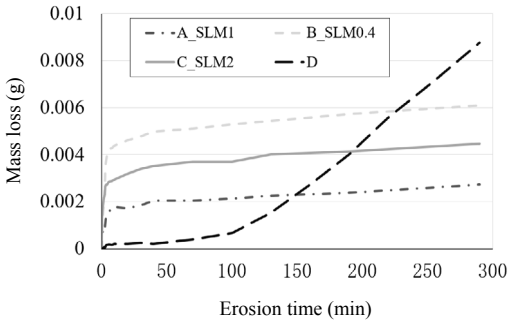

Fig. 14 Cumulative mass loss versus time for four samples
SLM1: standard scanning speed; SLM0.4: 0.4 times of the standard scanning speed; SLM2: 2 times of the standard scanning speed; D: wrought. Reprinted from (Zou et al., 2017), Copyright 2017, with permission from Elsevier

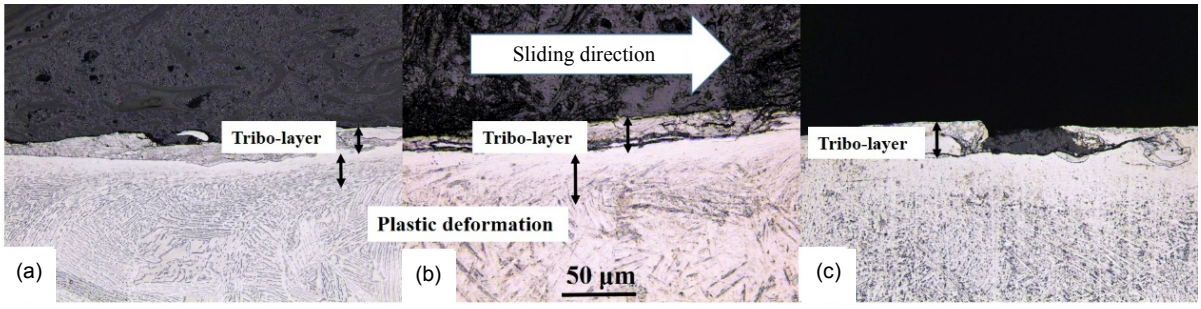

Fig. 13 Tribo-layers on CP (a), as-prepared SLM (b), and heat-treated SLM (c) samples. Reprinted from (Zhu et al., 2016b), Copyright 2016, with permission from Elsevier

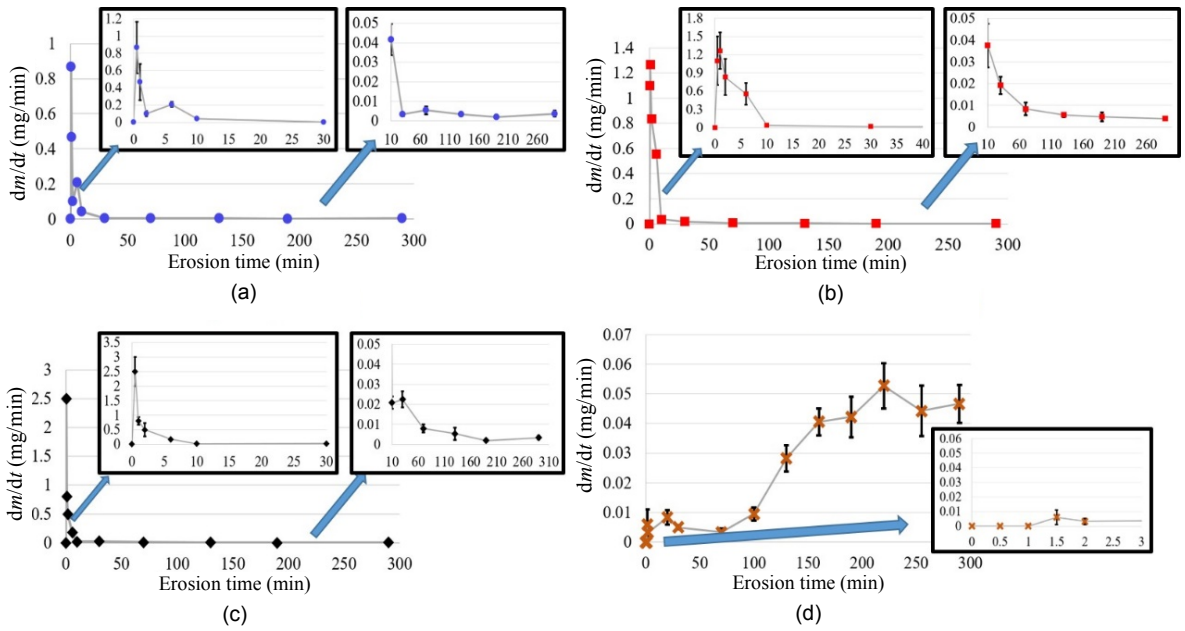

Fig. 15 Mass loss rate of four samples: (a) A_SLM1; (b) B_SLM0.4; (c) C_SLM2; (d) D. Reprinted from (Zou et al., 2017), Copyright 2017, with permission from Elsevier

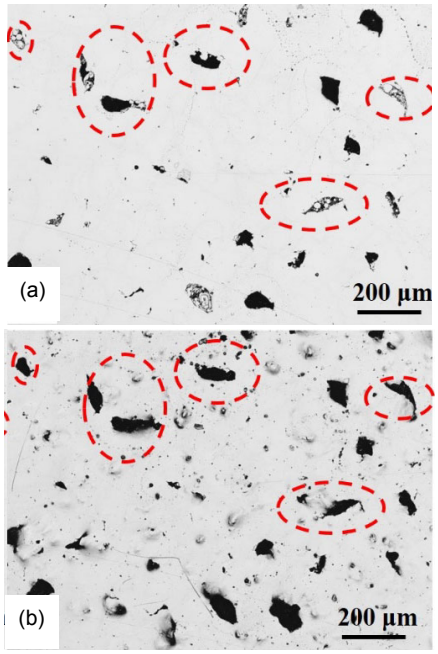

Fig. 16 Surface topography tracking of sample C_SLM2 observed at the original state (a) and after 30 s (b). Reprinted from (Zou et al., 2017), Copyright 2017, with permission from Elsevier

reasons for the high erosion resistance in the steady-state period. Laser scanning speeds affect the sample density and the number of pores, which further influence the maximum erosion rate. The one produced by the standard scanning speed gives the highest erosion resistance due to the highest densification and the least number of pores.

4.4 Corrosion

Corrosion can be defined as the degradation of a material due to a reaction with its environment. Corrosive wear refers to the damage caused by synergistic attack of wear and corrosion when wear occurs in a corrosive environment. Corrosive wear is related to another area termed "tribo-corrosion". We only describe some differences in corrosion behavior between the SLMed and the CP materials.

Dai et al. (2016a) compared the corrosion behavior of SLMed Ti-6Al-4V alloy with a commercial Grade 5 sample. Results indicated that the SLMed sample possessed poorer corrosion resistance than the Grade 5 sample due to the large amount of acicular α′ and less β-Ti phase in the microstructure. Dai et al. (2016b) also indicated that the building plane influenced the corrosion resistance. The *XY*-plane possesses a better corrosion resistance than the *XZ*-plane in HCl solution due to less α′ martensite and more β-Ti phase. The corrosion resistance can be improved by using Ti-TiB composites (Attar et al., 2014a). This is because tiny TiB and TiB_2 particles act as the

micro-cathode uniformly distributing in the titanium matrix. Anodic dissolution of the titanium matrix in the corrosion process is prominently facilitated in early stages, followed by rapid passivation on the surface. The corrosion behavior of aluminum alloy was studied by Prashanth et al. (2014) and Cabrini et al. (2016). Results indicated that the corrosion resistance of SLMed aluminum is similar to that of the cast sample. The size of the hard Si particles is crucial for corrosion behavior. Sun et al. (2013) studied the corrosion behavior of 316L stainless steel and found that the corrosion resistance between the SLMed sample and the standard 316L is similar. However, the SLMed steel suffers from a reduced breakdown potential and is more susceptible to pitting corrosion which is related to the porosity.

5 Discussion, future work, and concluding remarks

As can be seen from the above literature review, most studies were performed under dry conditions. The contact pressure ranges from below 1 MPa by face contacts to 1.9 GPa by point contacts. The sliding speeds range from 0.03 m/s to 1 m/s while the fretting frequency from 10 Hz to 50 Hz. Under such a wide range of contact conditions, the SLMed parts generally have higher wear resistance than the corresponding CP parts except for the results reported by Sun et al. (2013). In their work, poor wear resistance of the SLMed parts may be because of a relatively high porosity. The SLM processing parameters greatly influence density, hardness, and wear rates. It is widely accepted that a good combination of the SLM processing parameters improves the part densification, which further increases the wear resistance under dry conditions. A fully densified part benefits from fine and closely arranged grains, which lead to a high resistance against deformation compared to the CP parts. Poor densification generates pores and cracks, which further propagate under the severe contact conditions leading to material delamination and high wear.

However, many metal parts in industrial application are lubricated. The only studies available in the literature were performed under the boundary lubrication regime. In that case, direct metal-metal contact still dominates. According to those studies, near-full densified SLM parts (stainless steel and titanium alloy) have better wear performance than CP parts. This is mainly because of the SLM microstructure, as explained already. Hardness also contributes to the low wear rates since the SLMed parts are harder than the CP parts because of very fast heat conduction in the SLM process. A different tribo-layer is also noticed. Tribo-layers are of great importance because they change the contact from direct metal-metal contact to the contact between the metal and the tribo-layer. Further study is required for a better understanding of the formation and failure of tribo-layers on the surface of the SLMed parts.

However, research has been barely performed when a lubricant film is fully or partially formed. In that case, the influence of a lubricant film can outweigh that of the SLMed microstructures. Surface pores may positively influence the formation of the lubricating film. A similar case studied widely is surface texture. A surface with textures can reduce friction and wear under certain conditions due to extra lubrication and by acting as wear debris containers. Whether the pores have a positive influence on reducing friction and wear is a research question to be answered.

A new cavitation erosion behavior of SLMed AlSi10Mg was found and investigated. This study indicates that SLMed parts have high cavitation erosion resistance and the resistance can be further increased by reducing the surface pores. The conclusion can be used in fields where materials suffer from cavitation erosion such as hydraulics and aerospace. More research needs to be performed in order to confirm that the phenomenon does not solely belong to the aluminum alloy.

As indicated in the literature review, different combinations of the SLM processing parameters produce metal parts with pores in different sizes and morphologies. The interaction between pores and counterparts (or lubricant films) under various contact conditions is worth studying. The final step is to positively control the pores and microstructures of the SLMed materials to achieve low friction and wear by adjusting the SLM processing parameters.

Corrosion is mentioned without going deep into details in this paper. Some studies were performed and the results indicated that there is no remarkable

difference between the SLMed material and the same standard material. However, a systematic study is required since corrosive conditions greatly vary. In addition, as one aspect of tribology, friction is also crucial. There are many published articles that have measured the coefficient of friction of SLMed materials (Gu et al., 2011a, 2015; Gu, 2012; Kang, 2016; Bartolomeu et al., 2017). Since the topic of the paper is wear, friction behaviors of the SLMed materials can be investigated by another work.

In conclusion, SLMed materials generally have higher wear resistance than CP materials under dry, boundary lubrication, and cavitation erosion conditions mainly due to the fine grains and high hardness. On the other hand, a unique tribo-layer is also formed on the SLMed part under a boundary lubrication regime, and this protects the bulk material from plastic deformation. The SLM processing parameters are crucial for wear rates since a fully densified part usually has high wear resistance. However, more work needs to be performed to investigate the influence of pores on deforming and lubricating behaviors from dry conditions to different lubrication regimes. More importantly, mechanisms behind the wear behavior of the SLMed materials need to be understood to further positively control the SLM processing parameters to improve wear resistance. In that case, the application of the SLM technology can be greatly expanded to fabricate frictional pairs.

References

AlMangour B, Grzesiak D, Yang JM, 2016. Rapid fabrication of bulk-form TiB_2/316L stainless steel nanocomposites with novel reinforcement architecture and improved performance by selective laser melting. *Journal of Alloys and Compounds*, 680:480-493. https://doi.org/10.1016/j.jallcom.2016.04.156

AlMangour B, Grzesiak D, Yang JM, 2017a. In-situ formation of novel TiC-particle-reinforced 316L stainless steel bulk-form composites by selective laser melting. *Journal of Alloys and Compounds*, 706:409-418. https://doi.org/10.1016/j.jallcom.2017.01.149

AlMangour B, Grzesiak D, Yang JM, 2017b. Selective laser melting of TiB_2/316L stainless steel composites: the roles of powder preparation and hot isostatic pressing post-treatment. *Powder Technology*, 309:37-48. https://doi.org/10.1016/j.powtec.2016.12.073

Attar H, Bonisch M, Calin M, et al., 2014a. Comparative study of microstructures and mechanical properties of in situ Ti-TiB composites produced by selective laser melting, powder metallurgy, and casting technologies. *Journal of Materials Research*, 29(17):1941-1950. https://doi.org/10.1557/jmr.2014.122

Attar H, Calin M, Zhang LC, et al., 2014b. Manufacture by selective laser melting and mechanical behavior of commercially pure titanium. *Materials Science and Engineering: A*, 593:170-177. https://doi.org/10.1016/j.msea.2013.11.038

Attar H, Bönisch M, Calin M, et al., 2014c. Selective laser melting of in situ titanium-titanium boride composites: processing, microstructure and mechanical properties. *Acta Materialia*, 76:13-22. https://doi.org/10.1016/j.actamat.2014.05.022

Attar H, Prashanth KG, Chaubey AK, et al., 2015a. Comparison of wear properties of commercially pure titanium prepared by selective laser melting and casting processes. *Materials Letters*, 142:38-41. https://doi.org/10.1016/j.matlet.2014.11.156

Attar H, Prashanth KG, Zhang LC, et al., 2015b. Effect of powder particle shape on the properties of in situ Ti-TiB composite materials produced by selective laser melting. *Journal of Materials Science and Technology*, 31(10): 1001-1005. https://doi.org/10.1016/j.jmst.2015.08.007

Attar H, Lober H, Funk A, et al., 2015c. Mechanical behavior of porous commercially pure Ti and Ti-TiB composite materials manufactured by selective laser melting. *Materials Science and Engineering: A*, 625:350-356. https://doi.org/10.1016/j.msea.2014.12.036

Attar H, Ehtemam-Haghighi S, Kent D, et al., 2017. Nanoindentation and wear properties of Ti and Ti-TiB composite materials produced by selective laser melting. *Materials Science and Engineering: A*, 688:20-26. https://doi.org/10.1016/j.msea.2017.01.096

Bai Y, Gai X, Li S, et al., 2017. Improved corrosion behaviour of electron beam melted Ti-6Al-4V alloy in phosphate buffered saline. *Corrosion Science*, 123:289-296. https://doi.org/10.1016/j.corsci.2017.05.003

Bartolomeu F, Sampaio M, Carvalho O, et al., 2017. Tribological behavior of Ti6Al4V cellular structures produced by selective laser melting. *Journal of the Mechanical Behavior of Biomedical Materials*, 69:128-134. https://doi.org/10.1016/j.jmbbm.2017.01.004

Brandl E, Heckenberger U, Holzinger V, et al., 2012. Additive manufactured AlSi10Mg samples using selective laser melting (SLM): microstructure, high cycle fatigue, and fracture behavior. *Materials & Design*, 34:159-169. https://doi.org/10.1016/j.matdes.2011.07.067

Cabrini M, Lorenzi S, Pastore T, et al., 2016. Evaluation of corrosion resistance of Al-10Si-Mg alloy obtained by means of direct metal laser sintering. *Journal of Materials Processing Technology*, 231:326-335. https://doi.org/10.1016/j.jmatprotec.2015.12.033

Chen HY, Gu DD, 2016. Effect of metallurgical defect and phase transition on geometric accuracy and wear resistance of iron-based parts fabricated by selective laser melting. *Journal of Materials Research*, 31(10):1477-

1490.
https://doi.org/10.1557/jmr.2016.132

Chen Y, Zhang JX, Dai NW, et al., 2017. Corrosion behaviour of selective laser melted Ti-TiB biocomposite in simulated body fluid. *Electrochimica Acta*, 232:89-97.
https://doi.org/10.1016/j.electacta.2017.02.112

Cherry JA, Davies HM, Mehmood S, et al., 2014. Investigation into the effect of process parameters on microstructural and physical properties of 316L stainless steel parts by selective laser melting. *The International Journal of Advanced Manufacturing Technology*, 76(5-8):869-879.
https://doi.org/10.1007/s00170-014-6297-2

Dai NW, Zhang LC, Zhang JX, et al., 2016a. Corrosion behavior of selective laser melted Ti-6Al-4V alloy in NaCl solution. *Corrosion Science*, 102:484-489.
https://doi.org/10.1016/j.corsci.2015.10.041

Dai NW, Zhang LC, Zhang JX, et al., 2016b. Distinction in corrosion resistance of selective laser melted Ti-6Al-4V alloy on different planes. *Corrosion Science*, 111:703-710.
https://doi.org/10.1016/j.corsci.2016.06.009

Ehtemam-Haghighi S, Prashanth KG, Attar H, et al., 2016. Evaluation of mechanical and wear properties of Ti-*x*Nb-7Fe alloys designed for biomedical applications. *Materials & Design*, 111:592-599.
https://doi.org/10.1016/j.matdes.2016.09.029

Ehtemam-Haghighi S, Cao GH, Zhang LC, 2017. Nanoindentation study of mechanical properties of Ti based alloys with Fe and Ta additions. *Journal of Alloys and Compounds*, 692:892-897.
https://doi.org/10.1016/j.jallcom.2016.09.123

El Kadiri H, Wang L, Horstemeyer MF, et al., 2008. Phase transformations in low-alloy steel laser deposits. *Materials Science and Engineering: A*, 494(1-2):10-20.
https://doi.org/10.1016/j.msea.2007.12.011

Gu DD, 2012. Densification behavior, microstructure evolution, and wear performance of selective laser melting processed commercially pure titanium. *Acta Materialia*, 60(9):3849-3860.
https://doi.org/10.1016/j.actamat.2012.04.006

Gu DD, Shen YF, 2007. Balling phenomena during direct laser sintering of multi-component Cu-based metal powder. *Journal of Alloys and Compounds*, 432(1-2):163-166.
https://doi.org/10.1016/j.jallcom.2006.06.011

Gu DD, Hong C, Meng GB, 2011a. Densification, microstructure, and wear property of in situ titanium nitride-reinforced titanium silicide matrix composites prepared by a novel selective laser melting process. *Metallurgical and Materials Transactions A*, 43(2):697-708.
https://doi.org/10.1007/s11661-011-0876-8

Gu DD, Hagedorn YC, Meiners W, et al., 2011b. Selective laser melting of in-situ TiC/Ti_5Si_3 composites with novel reinforcement architecture and elevated performance. *Surface and Coatings Technology*, 205(10):3285-3292.
https://doi.org/10.1016/j.surfcoat.2010.11.051

Gu DD, Meiners W, Wissenbach K, et al., 2012. Laser additive manufacturing of metallic components: materials, processes and mechanisms. *International Materials Reviews*, 57(3):133-164.
https://doi.org/10.1179/1743280411Y.0000000014

Gu DD, Wang HQ, Dai DH, et al., 2015. Densification behavior, microstructure evolution, and wear property of TiC nanoparticle reinforced AlSi10Mg bulk-form nanocomposites prepared by selective laser melting. *Journal of Laser Applications*, 27(S1):S17003.
https://doi.org/10.2351/1.4870877

Hedberg YS, Qian B, Shen Z, et al., 2014. In vitro biocompatibility of CoCrMo dental alloys fabricated by selective laser melting. *Dental Materials*, 30(5):525-534.
https://doi.org/10.1016/j.dental.2014.02.008

Jägle EA, Choi PP, van Humbeeck J, et al., 2014. Precipitation and austenite reversion behavior of a maraging steel produced by selective laser melting. *Journal of Materials Research*, 29(17):2072-2079.
https://doi.org/10.1557/jmr.2014.204

Jia QB, Gu DD, 2014. Selective laser melting additive manufacturing of Inconel 718 superalloy parts: densification, microstructure and properties. *Journal of Alloys and Compounds*, 585:713-721.
https://doi.org/10.1016/j.jallcom.2013.09.171

Johnson KL, 1985. Contact Mechanics. Cambridge University Press, Cambridge, UK.
https://doi.org/10.1017/CBO9781139171731

Kang N, 2016. Wear behavior and microstructure of hypereutectic Al-Si alloys prepared by selective laser melting. *Applied Surface Science*, 378:142-149.
https://doi.org/10.1016/j.apsusc.2016.03.221

Kang N, Coddet P, Liao H, et al., 2016. Wear behavior and microstructure of hypereutectic Al-Si alloys prepared by selective laser melting. *Applied Surface Science*, 378:142-149.
https://doi.org/10.1016/j.apsusc.2016.03.221

Kempen K, Thijs L, Humbeeck JV, et al., 2012. Mechanical properties of AlSi10Mg produced by selective laser melting. *Physics Procedia*, 39:439-446.
https://doi.org/10.1016/j.phpro.2012.10.059

Koike M, Greer P, Owen K, et al., 2011. Evaluation of titanium alloys fabricated using rapid prototyping technologies-electron beam melting and laser beam melting. *Materials*, 4(12):1776-1792.
https://doi.org/10.3390/ma4101776

Körner C, Bauereib A, Attar E, 2013. Fundamental consolidation mechanisms during selective beam melting of powders. *Modelling and Simulation in Materials Science and Engineering*, 21(8):085011.
https://doi.org/10.1088/0965-0393/21/8/085011

Kumar S, Kruth JP, 2008. Wear performance of SLS/SLM materials. *Advanced Engineering Materials*, 10(8):750-753.
https://doi.org/10.1002/adem.200800075

Leuders S, Thöne M, Riemer A, et al., 2013. On the mechanical behaviour of titanium alloy TiAl6V4 manufactured

by selective laser melting: fatigue resistance and crack growth performance. *International Journal of Fatigue*, 48:300-307. https://doi.org/10.1016/j.ijfatigue.2012.11.011

Li XP, Kang CW, Huang H, et al., 2014. Selective laser melting of an Al86Ni6Y4.5Co2La1.5 metallic glass: processing, microstructure evolution and mechanical properties. *Materials Science and Engineering: A*, 606(2):370-379. https://doi.org/10.1016/j.msea.2014.03.097

Li YL, Gu DD, 2014. Parametric analysis of thermal behavior during selective laser melting additive manufacturing of aluminum alloy powder. *Materials & Design*, 63(2):856-867. https://doi.org/10.1016/j.matdes.2014.07.006

Liu YJ, Li XP, Zhang LC, et al., 2015. Processing and properties of topologically optimised biomedical Ti-24Nb-4Zr-8Sn scaffolds manufactured by selective laser melting. *Materials Science and Engineering: A*, 642:268-278. https://doi.org/10.1016/j.msea.2015.06.088

Liu YJ, Li SJ, Wang HL, et al., 2016. Microstructure, defects and mechanical behavior of β-type titanium porous structures manufactured by electron beam melting and selective laser melting. *Acta Materialia*, 113:56-67. https://doi.org/10.1016/j.actamat.2016.04.029

Liu YJ, Wang HL, Li SJ, et al., 2017. Compressive and fatigue behavior of beta-type titanium porous structures fabricated by electron beam melting. *Acta Materialia*, 126:58-66. https://doi.org/10.1016/j.actamat.2016.12.052

Manfredi D, Calignano F, Krishnan M, et al., 2013. From powders to dense metal parts: characterization of a commercial AlSiMg alloy processed through direct metal laser sintering. *Materials*, 6(3):856-869. https://doi.org/10.3390/ma6030856

Prashanth KG, Debalina B, Wang Z, et al., 2014. Tribological and corrosion properties of Al–12Si produced by selective laser melting. *Journal of Materials Research*, 29(17): 2044-2054. https://doi.org/10.1557/jmr.2014.133

Prashanth KG, Shahabi HS, Attar H, et al., 2015. Production of high strength Al85Nd8Ni5Co2 alloy by selective laser melting. *Additive Manufacturing*, 6:1-5.

Prashanth KG, Scudino S, Chaubey AK, et al., 2016. Processing of Al-12Si-TNM composites by selective laser melting and evaluation of compressive and wear properties. *Journal of Materials Research*, 31(1):55-65. https://doi.org/10.1557/jmr.2015.326

Qiu C, Panwisawas C, Ward M, et al., 2015. On the role of melt flow into the surface structure and porosity development during selective laser melting. *Acta Materialia*, 96:72-79. https://doi.org/10.1016/j.actamat.2015.06.004

Riemer A, Leuders S, Thone M, et al., 2014. On the fatigue crack growth behavior in 316L stainless steel manufactured by selective laser melting. *Engineering Fracture Mechanics*, 120(4):15-25. https://doi.org/10.1016/j.engfracmech.2014.03.008

Rong T, Gu DD, Shi Q, et al., 2016. Surface & coatings technology effects of tailored gradient interface on wear properties of WC/Inconel 718 composites using selective laser melting. *Surface & Coatings Technology*, 307:418-427. https://doi.org/10.1016/j.surfcoat.2016.09.011

Scudino S, Unterdorfer C, Prashanth KG, et al., 2015. Additive manufacturing of Cu-10Sn bronze. *Materials Letters*, 156:202-204. https://doi.org/10.1016/j.matlet.2015.05.076

Simonelli M, Tuck C, Aboulkhair NT, et al., 2015. A study on the laser spatter and the oxidation reactions during selective laser melting of 316L stainless steel, Al-Si10-Mg, and Ti-6Al-4V. *Metallurgical and Materials Transactions A*, 46(9):3842-3851. https://doi.org/10.1007/s11661-015-2882-8

Sun Y, Moroz A, Alrbaey K, 2013. Sliding wear characteristics and corrosion behaviour of selective laser melted 316L stainless steel. *Journal of Materials Engineering and Performance*, 23(2):518-526. https://doi.org/10.1007/s11665-013-0784-8

Sun Z, Tan X, Shu BT, et al., 2016. Selective laser melting of stainless steel 316L with low porosity and high build rates. *Materials & Design*, 104:197-204. https://doi.org/10.1016/j.matdes.2016.05.035

Thijs L, Verhaeghe F, Craeghs T, et al., 2010. A study of the microstructural evolution during selective laser melting of Ti-6Al-4V. *Acta Materialia*, 58(9):3303-3312. https://doi.org/10.1016/j.actamat.2010.02.004

Thijs L, Kempen K, Kruth JP, et al., 2013. Fine-structured aluminium products with controllable texture by selective laser melting of pre-alloyed AlSi10Mg powder. *Acta Materialia*, 61(5):1809-1819. https://doi.org/10.1016/j.actamat.2012.11.052

Uriondo A, Esperon-Miguez M, Perinpanayagam S, 2015. The present and future of additive manufacturing in the aerospace sector: a review of important aspects. *Proceedings of the Institution of Mechanical Engineers, Part G: Journal of Aerospace Engineering*, 229(11):2132-2147. https://doi.org/10.1177/0954410014568797

van Beek A, 2006. Advanced Engineering Design. TU Delft, the Netherlands, p.87-136.

Vrancken B, Thijs L, Kruth JP, et al., 2012. Heat treatment of Ti6Al4V produced by selective laser melting: microstructure and mechanical properties. *Journal of Alloys and Compounds*, 541:177-185. https://doi.org/10.1016/j.jallcom.2012.07.022

Vrancken B, Thijs L, Kruth JP, et al., 2014. Microstructure and mechanical properties of a novel β titanium metallic composite by selective laser melting. *Acta Materialia*, 68(15):150-158. https://doi.org/10.1016/j.actamat.2014.01.018

Wang XQ, Chou K, 2017. Electron backscatter diffraction analysis of Inconel 718 parts fabricated by selective laser

melting additive manufacturing. *Journal of Materials*, 69(2):402-408.

Wu SQ, Lu YJ, Gan YL, et al., 2016. Microstructural evolution and microhardness of a selective-laser-melted Ti-6Al-4V alloy after post heat treatments. *Journal of Alloys and Compounds*, 672:643-652. https://doi.org/10.1016/j.jallcom.2016.02.183

Zhang B, Dembinski L, Coddet C, 2013. The study of the laser parameters and environment variables effect on mechanical properties of high compact parts elaborated by selective laser melting 316L powder. *Materials Science and Engineering: A*, 584(6):21-31. https://doi.org/10.1016/j.msea.2013.06.055

Zhang LC, Attar H, 2016. Selective laser melting of titanium alloys and titanium matrix composites for biomedical applications: a review. *Advanced Engineering Materials*, 18(4):463-475. https://doi.org/10.1002/adem.201500419

Zhang LC, Klemm D, Eckert J, et al., 2011. Manufacture by selective laser melting and mechanical behavior of a biomedical Ti-24Nb-4Zr-8Sn alloy. *Scripta Materialia*, 65(1):21-24. https://doi.org/10.1016/j.scriptamat.2011.03.024

Zheng L, Neville A, Gledhill A, et al., 2010. An experimental study of the corrosion behavior of nickel tungsten carbide in some water-glycol hydraulic fluids for subsea applications. *Journal of Materials Engineering and Performance*, 19(1):90-98. https://doi.org/10.1007/s11665-009-9416-8

Zhou X, Liu X, Zhang D, et al., 2015. Balling phenomena in selective laser melted tungsten. *Journal of Materials Processing Technology*, 222:33-42. https://doi.org/10.1016/j.jmatprotec.2015.02.032

Zhu Y, Zou J, Chen X, et al., 2016a. Tribology of selective laser melting processed parts: stainless steel 316L under lubricated conditions. *Wear*, 350-351:46-55. https://doi.org/10.1016/j.wear.2016.01.004

Zhu Y, Chen X, Zou J, et al., 2016b. Sliding wear of selective laser melting processed Ti6Al4V under boundary lubrication conditions. *Wear*, 368-369:485-495. https://doi.org/10.1016/j.wear.2016.09.020

Zou J, Zhu Y, Pan M, et al., 2017. A study on cavitation erosion behavior of AlSi10Mg fabricated by selective laser melting (SLM). *Wear*, 376-377:496-506. https://doi.org/10.1016/j.wear.2016.11.031

中文概要

题　目：选区激光熔化成形件磨损特性综述

概　要：通过对文献的综述，本文总结了已有的选区激光熔化成形件的磨损特性研究，并提出了未来的研究方向，为该技术成形摩擦副的推广提供参考。本文通过干磨、边界润滑下的磨损、腐蚀以及冲蚀四个方面介绍了已有研究。总体来看，选区激光熔化成形件得益于均匀细晶，高致密度成形件的磨损率普遍低于传统制造件，然而孔隙的出现将降低成形件的抗磨性能。未来的研究内容主要包括孔隙对润滑的影响规律及其机理，以及如何通过主动控制激光工艺参数提高选区激光熔化成形件的抗磨能力。

关键词：选区激光熔化；磨损；增材制造；润滑；孔隙